Chapter 5

Thermodynamic Property Study on the Complexes of Rare-Earth Elements with Amino Aids

Zhi Cheng Tan, Quan Shi, Xue Chuan Lv and Bei Ping Liu

Additional information is available at the end of the chapter

http://dx.doi.org/10.5772/intechopen.69473

Abstract

In this chapter, the following three rare-earth complexes with amino acids, Eu(Glu)$(Im)_5(ClO_4)_3 \cdot 3HClO_4 \cdot 6H_2O$, $Nd(Gly)_2Cl_3 \cdot 3H_2O$, and $La(Glu)(Im)_6(ClO_4)_3 \cdot 4HClO_4 \cdot 4H_2O$, are synthesized and characterized by element analysis, infrared (IR) spectrum, and x-ray diffraction (XRD) analysis. The thermodynamic property studies on these complexes are performed. For the first one, $Eu(Glu)(Im)_5(ClO_4)_3 \cdot 3HClO_4 \cdot 6H_2O$, the low temperature heat capacity, phase transition, and thermodynamic functions are determined by adiabatic calorimetry. For the second one, $Nd(Gly)_2Cl_3 \cdot 3H_2O$, the molar dissolution enthalpy and standard molar enthalpy of formation are determined by isoperibol solution reaction calorimetry. For the third one, $La(Glu)(Im)_6(ClO_4)_3 \cdot 4HClO_4 \cdot 4H_2O$, the microcalorimetry is used to investigate the interaction between the complex and the *Escherichia coli* DH5α to elucidate the biological effects of the complex.

Keywords: complexes of rare-earth elements, amino acids, adiabatic calorimetry (AC), solution reaction calorimetry, microcalorimetry, thermal analysis, thermodynamic properties, heat capacity, phase transition

1. Introduction

Rare-earth (RE) elements and their compounds have been extensively investigated in last several decades, because of their important significance in sciences and the growing practical applications in industries. New frontiers concerned with RE science and technology are increasingly and rapidly developed.

It is well know that China is the country richest in RE minerals all over the world. In order to sufficiently develop and effectively utilize the RE resources, the industries concerned were in urgent need of huge numbers of basic data of RE compounds. Undoubtedly, the thermodynamic property data are absolutely necessary for the study and application of rare-earth

compounds. As one part of Chinese national research projects for rare-earth science and technology, in the period of 1990–2006, our Thermochemistry Laboratory in cooperation with Microcalorimetry Research Center of Osaka University well successfully completed the research project "low temperature heat capacity and thermodynamic properties of a series of rare-earth isothiocyanate hydrates, $RE(NCS)_3 \cdot nH_2O$ (RE = La,Ce,Pr,Nd,Sm,Gd,Yb,Y)." The research results concerned were published in international journals [1–4].

Rare-earth elements have found their applications in many areas nowadays; because of their unique properties, they have been introduced into microfertilizer, pesticide, and antibacterial agent. Accompanying these applications, rare-earth elements inevitably spread into the food chain, the biological chain, and then into the bodies of human beings. This leads people to care about and study the influence and the long-term effect of rare-earth elements on themselves. Rare-earth complexes formed with amino acid were then synthesized for this purpose, because amino acid is the basic unit comprising protein and enzyme, the fundamental and functional materials in the bodies of human beings and animals. In the last 30 years, more than 200 kinds of these complexes were synthesized, and about 50 kinds among them had their own crystallograms. However, the thermodynamic property data of these complexes were seldom reported. As we all well know, only with these data we can quantitatively describe their characteristics in terms of the energetics, for example, stable forms in different temperature range, melting process, thermal anomaly, and so on. Comparisons of these data for a series of complexes comprised by the same RE (or ligands) with different ligands (or RE) may enable us to have a deeper understanding of their properties.

Rare-earth complex coordinated with amino acids possesses many unique physiological and biochemical effects. In 1975, Anghileri et al. reported for the first time that $La(Gly)_3Cl_3 \cdot 3H_2O$ was antineoplastic [5]. Since then, the rare-earth complexes coordinated with amino acids have been synthesized and studied intensively by a variety of methods [6–10]. Nowadays, the applications of rare-earth complexes with amino acids have expanded into the fields of medicine, biology, and agriculture more widely. However, the fundamental thermodynamic property data of these complexes have rarely been reported yet, especially the data of low temperature heat capacity and standard thermodynamic functions, and standard enthalpy of formation, although these data are significant for the further applications of the rare-earth complex with amino acids.

Based on previous work about thermodynamic study of rare-earth isothiocyanate hydrates, our thermochemistry laboratory in cooperation with several national academic groups has intensively contributed to this effort for thermodynamic property studies on rare-earth complexes with amino acids, and 28 academic papers concerned with this research project have been published [11–38].

In this chapter, we present the following three papers to report our recent research results and describe in detail the modern advanced experimental calorimetric techniques used for thermodynamic property studies of rare-earth complexes.

1. Thermodynamic properties of rare-earth complex with amino acid: $Eu(Glu)(Im)_5(ClO_4)_3 \cdot 3HClO_4 \cdot 6H_2O$

2. Thermodynamic study on rare-earth complex of neodymium with glycine: $Nd(Gly)_2Cl_3 \cdot 3H_2O$

3. Microcalorimetric study on biological effect of rare-earth complex with amino acid: $La(Glu)(Im)_6(ClO_4)_3 \cdot 4HClO_4 \cdot 4H_2O$

2. Thermodynamic properties of rare-earth complex with amino acid: $Eu(Glu)(Im)_5(ClO_4)_3 \cdot 3HClO_4 \cdot 6H_2O$

2.1. Experiment

2.1.1. Synthesis and characterization of the complex

The complex, $Eu(Glu)(Im)_5(ClO_4)_3 \cdot 3HClO_4 \cdot 6H_2O$, was synthesized according to the procedures mentioned below. All starting materials used for the synthesis are the analytical reagents purchased from the Beijing Chemical Reagent Co. The rare-earth oxide (Eu_2O_3) was dissolved in an excess amount of perchloric acid (1:1), and the concentration of the solution was determined by ethylene diamine tetraacetic acid (EDTA) titration analysis. Then, solid L-Glutamic acid was added to the solution in molar ratio of Eu^{3+}:Glu = 1:1. After the pH value of the reaction mixture was carefully adjusted to about 4.0 by slow addition of NaOH solution, imidazole was added in molar ratio of Eu^{3+}:Glu:Im = 1:1:5. The solution was stirred for a further 2 h in flask. The solution was transferred to the culture dish, and the culture dish was sealed using preservative film with many tiny holes stabbed using needle. The culture dish was placed in a desiccator using phosphorus pentoxide as the desiccant. The complex formed slowly in the solution and was taken out of the solution for analysis.

An elemental analysis apparatus (Model PE-2400 II, USA) was used to measure the C, H, N of the complex, and Eu was determined by EDTA titration analysis. The Cl amount in ClO_4^- of the complex was determined by the ion chromatography (Waters Alliance® 2695 System with the Waters Conductivity Detector and Waters Micromass® Quattro micro™ Mass Spectrometer). The experimental values are: Eu (11.60%) (mass fraction), C (17.794%), N (11.4093%), H (3.304%), and Cl (15.665%), which are close to the theoretical values, Eu (11.2792%), C (17.8293%), N (11.4358%), H (3.2917%), and Cl (15.789%). The sample formula was determined to be $Eu(Glu)(Im)_5\ (ClO_4)_3 \cdot 3HClO_4 \cdot 6H_2O$.

Infrared spectra of the complex and L-Glutamic acid were obtained through KBr pellets at room temperature using a Bruker Tensor 27-IR spectrophotometer. The infrared spectrum of the complex was shown in **Figure 1**. Compared with the IR spectrum of L-Glutamic acid, the νs (carboxyl) band of the complex shifted from 1410 cm^{-1} to higher wave numbers (1431 cm^{-1}), which shows that the carboxyl groups of the ligand have been coordinated to the metal ion [39]. The special absorptions of $-NH_2$ shifted from 3050 to 3240 cm^{-1} (ν -NH), from 2750 to 2740 cm^{-1} (ν -NH), and from 1560 to 1562 cm^{-1} (δNH_2^+), because a hydrogen bond formed in the complex. The spectrum also shows the wide peak symmetrical resonance frequencies, νs (N-H), shifted from 3286 to 3425 cm^{-1} down to 3166 to 3098 cm^{-1}, which is evidence of the

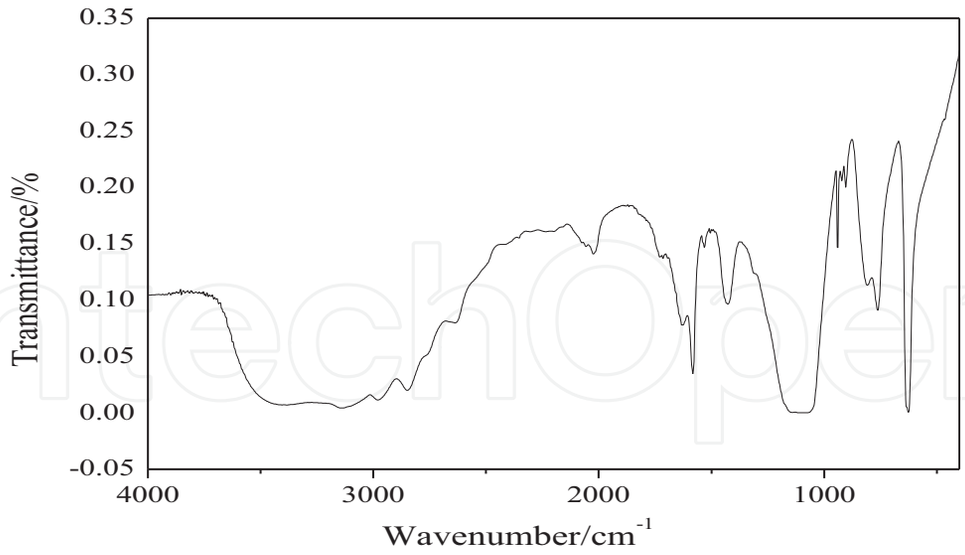

Figure 1. Infrared spectrum of the complex.

coordination of imidazole molecules [40]. A broad absorption band for ν (hydroxyl) appearing at 3400 cm^{-1} shows the presence of water molecules in the complex.

Powder X-ray diffraction (XRD) patterns were recorded using Rigaku D/Max 3400 X with Cu Kα radiation at 0.02 steps per second in angle range 2θ = 5–90, and the results were shown in **Figure 2**. Judging from the shape and number of the peak in the patterns, the sample was a kind of complex with single phase.

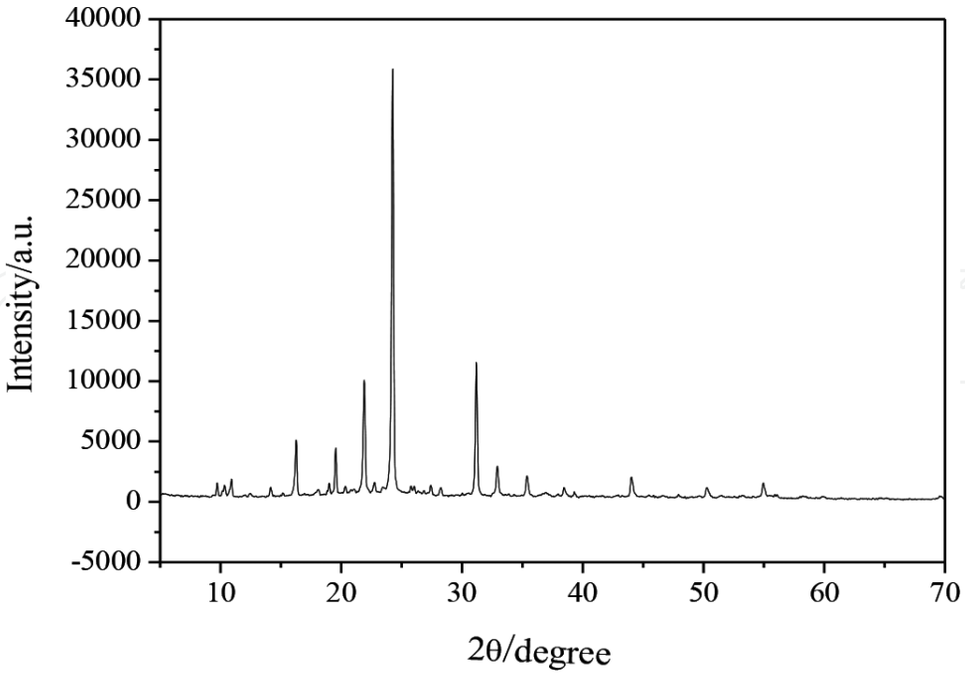

Figure 2. Powder X-ray diffraction patterns of complex.

2.1.2. Adiabatic calorimetry

Adiabatic calorimetry is the most accurate approach to obtain the heat capacity data. In the present study, heat capacity measurements were carried out by a high-precision automatic adiabatic calorimeter over the temperature range of 80–350 K. The adiabatic calorimeter was established by Thermochemistry Laboratory of Dalian Institute of Chemical Physics, Chinese Academy of Sciences in PR China. The structure and principle of the adiabatic calorimeter have been described in detail elsewhere [41]. The schematic diagram of the adiabatic calorimeter is shown in **Figure 3**. Briefly, the automatic adiabatic calorimeter is mainly composed of a sample cell, a miniature platinum resistance thermometer, an electric heater, the inner and outer adiabatic shields, two sets of six-junction chromel-constantan thermopiles installed between the calorimetric cell and the inner shield and between the inner and the outer shields, respectively, and a high vacuum can. The working temperature range is 78–400 K and, if necessary, it can be cooled by liquid nitrogen. The heat capacity measurements were conducted by the standard procedure of intermittently heating the sample and alternately measuring the temperature. The heating rate and the temperature increments of the experimental points were generally controlled at 0.1–0.4 $K \cdot min^{-1}$ and at 1–4 K, respectively, during the whole experimental process. The heating duration was 10 min, and the temperature drift rates of the sample cell measured in an equilibrium period were kept within 10^{-3}–10^{-4} $K \cdot min^{-1}$ during the acquisition of heat capacity data. In order to verify the reliability of the adiabatic calorimeter, the molar heat capacities $C_{p,m}$ of the Standard Reference Material (SRM-720) (α-Al_2O_3) were measured in the range of 78–400 K. The deviation of our calibration data from those of NIST [42] was within ±0.1% (standard uncertainty). In the present study, the mass of the complex, $Eu(Glu)(Im)_5(ClO_4)_3 \cdot 3HClO_4 \cdot 6H_2O$, used for heat capacity measurement was 2.0352 g.

The result of heat capacity measurement of the complex was listed in **Table 1** and shown in **Figure 4**.

2.1.3. Other thermal analysis

A differential scanning calorimeter (DSC−141, SETARAM, France) was used to perform the thermal analysis of $Eu(Glu)(Im)_5(ClO_4)_3 \cdot 3HClO_4 \cdot 6H_2O$. In the range 100–300 K, liquid nitrogen was used as cryogen. In the range 300–700 K, nitrogen gas was taken as protective gas with flow rate of 50 $cm^3 \cdot min^{-1}$, at the heating rate of 10 $K \cdot min^{-1}$. The masses of the samples used in the above two experiments were 4.03 and 4.26 mg, respectively.

Two aluminum crucibles were used and the reference crucible was empty. The calibrations for the temperature and heat flux of the calorimeter were performed prior to the experimental measurements of the sample. The temperature scale was calibrated by measuring the melting points of Hg, In, Sn, Pb, and Zn, at different heating rates, and the heat flux was calibrated by the Joule effect. Measurements of the melting temperature and the enthalpy of fusion of benzoic acid (NIST, Standard Reference Material 39i) were performed in the laboratory to check the accuracy of the instrument.

The result of DSC measurement was shown in **Figure 5**.

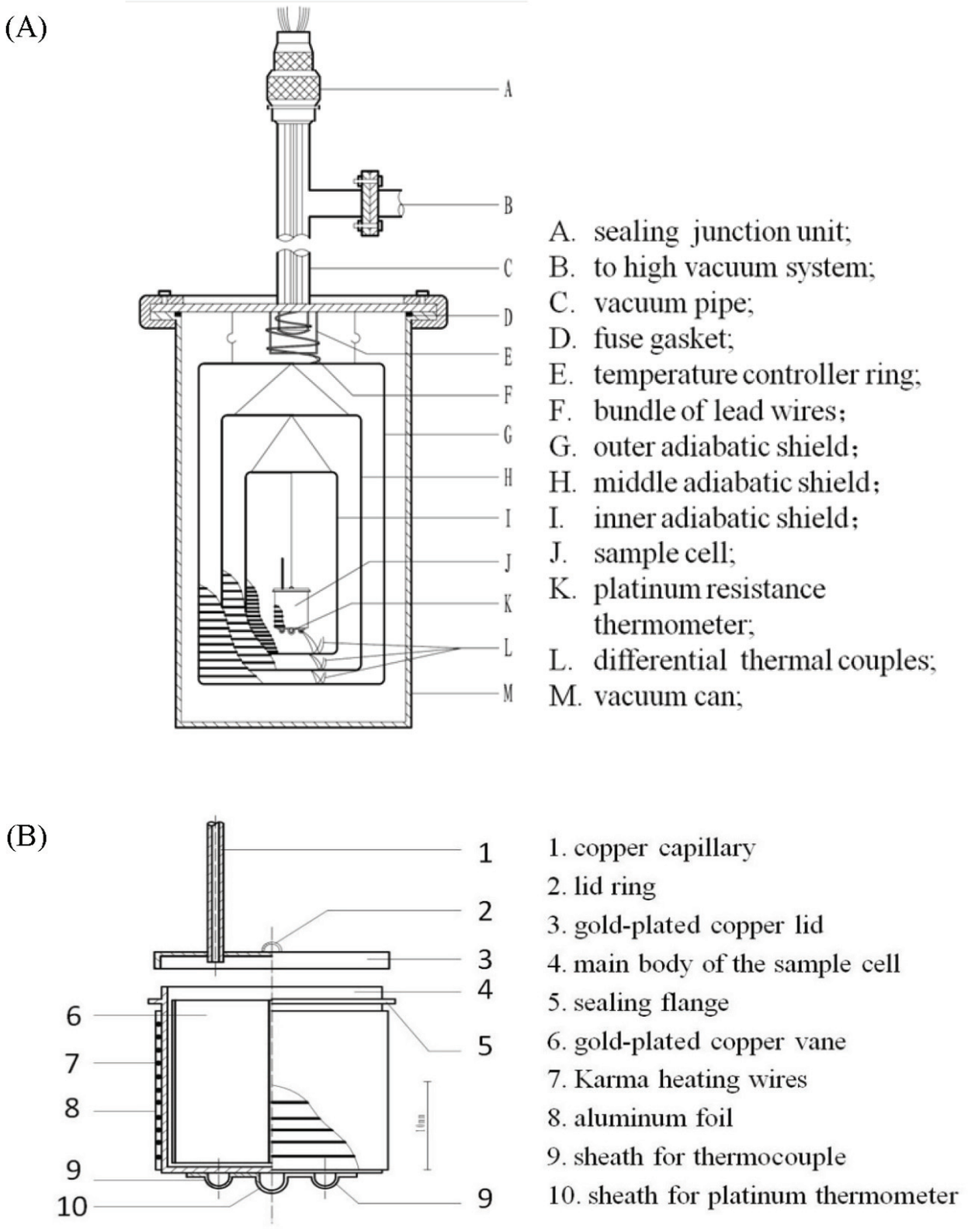

Figure 3. (A) Schematic diagram of main body of the adiabatic calorimeter. (B) Schematic diagram of sample cell of the adiabatic calorimeter.

T/K	$C_{p,m}$/kJ^{-1}·mol^{-1}	T/K	$C_{p,m}$/kJ^{-1}·mol^{-1}
80.809	919.23	216.99	2245.5
85.210	937.21	220.72	2147.5
89.334	959.77	224.63	2043.8
92.891	985.26	228.55	1900.4
96.695	999.58	232.60	2160.4
100.86	1023.5	236.58	2483.0
103.43	1041.7	240.60	2787.8
107.12	1059.7	244.18	4772.0
112.49	1090.3	246.08	11808.8
116.85	1120.2	252.57	2262.7
120.68	1140.2	258.60	2282.7
124.34	1163.4	262.37	2297.0
128.48	1187.6	266.06	2302.0
132.40	1209.4	269.69	2305.4
136.47	1242.6	273.60	2316.5
140.42	1263.1	277.58	2330.1
144.39	1284.7	281.39	2336.3
148.49	1308.0	285.46	2355.6
152.58	1334.7	289.26	2377.3
156.48	1359.5	293.34	2416.1
160.77	1383.9	297.43	2444.2
164.78	1412.6	301.37	2490.8
168.80	1439.5	305.18	2526.2
172.87	1465.4	309.23	2571.8
176.80	1488.0	313.12	2611.6
180.71	1512.7	316.85	2661.0
184.90	1542.9	319.85	2721.8
188.89	1577.1	324.82	2779.0
192.76	1610.9	328.77	2842.9
196.79	1644.1	332.78	2906.9
200.75	1681.2	336.67	2974.1
204.67	1728.7	340.52	3051.9
208.78	1788.1	344.52	3126.9
212.99	2025.9	348.77	3209.9

Table 1. Experimental molar heat capacity of the complex from 80 to 350 K at pressure p = 0.1 MPa.

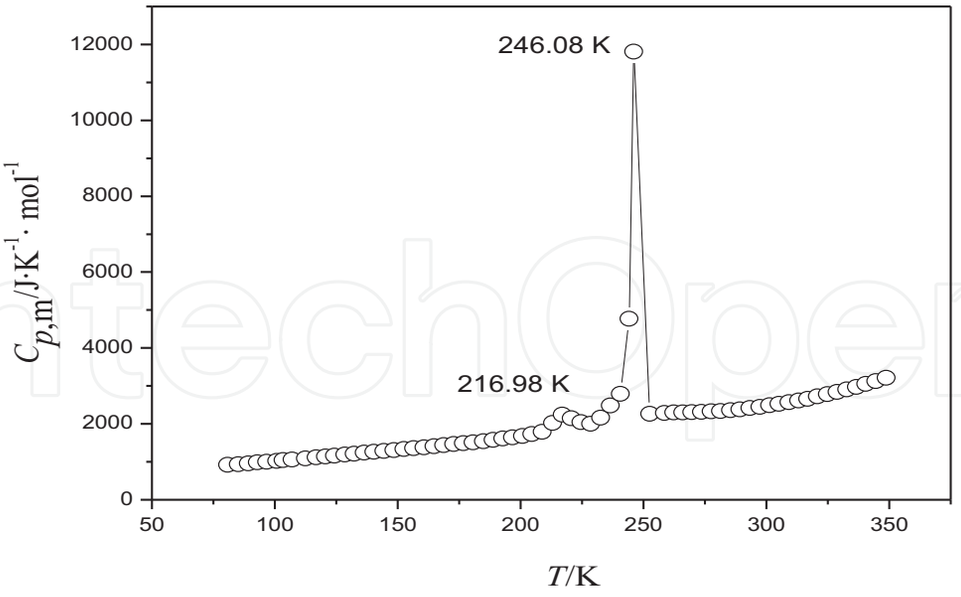

Figure 4. Experimental molar heat capacities as a function of temperature for the complex from 80 to 350 K.

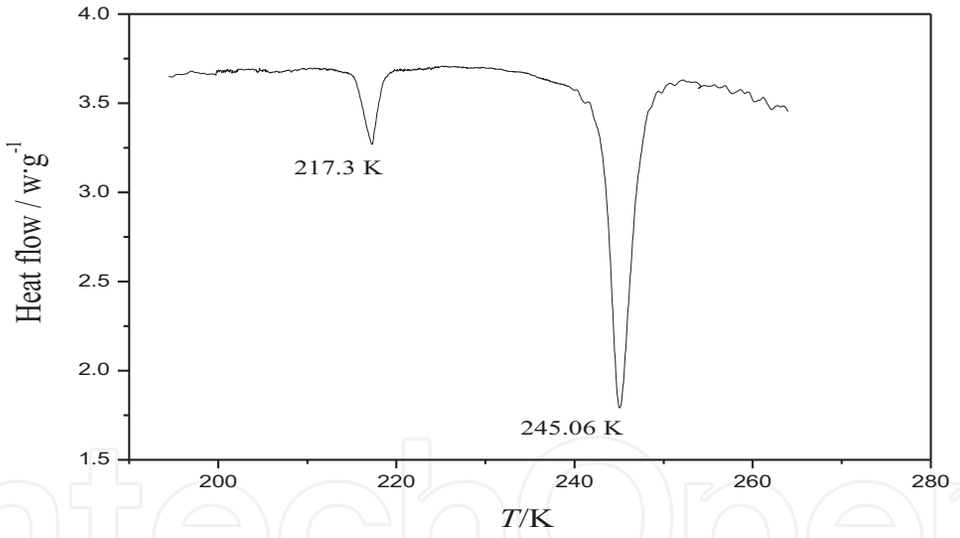

Figure 5. DSC curve of the complex from 200 to 270 K.

The thermogravimetric (TG) measurement of the complex was carried out by a TG analyzer (Model: setsys 16/18 from Setaram Company, France) at the heating rate of 10 K·min^{-1} under nitrogen atmosphere (99.999%), with flow rate of 65 cm^3·min^{-1}. The mass of the sample used in the experiment was 6.3 mg. Two Al_2O_3 crucibles with capacity of 100 μL were used for sample and empty cell, respectively. The calibration of TG analyzer was performed by the SRM in thermal analysis, $CaC_2O_4·H_2O$(s).

The result of TG measurement of the complex was shown in **Figures 6** and **7**, respectively.

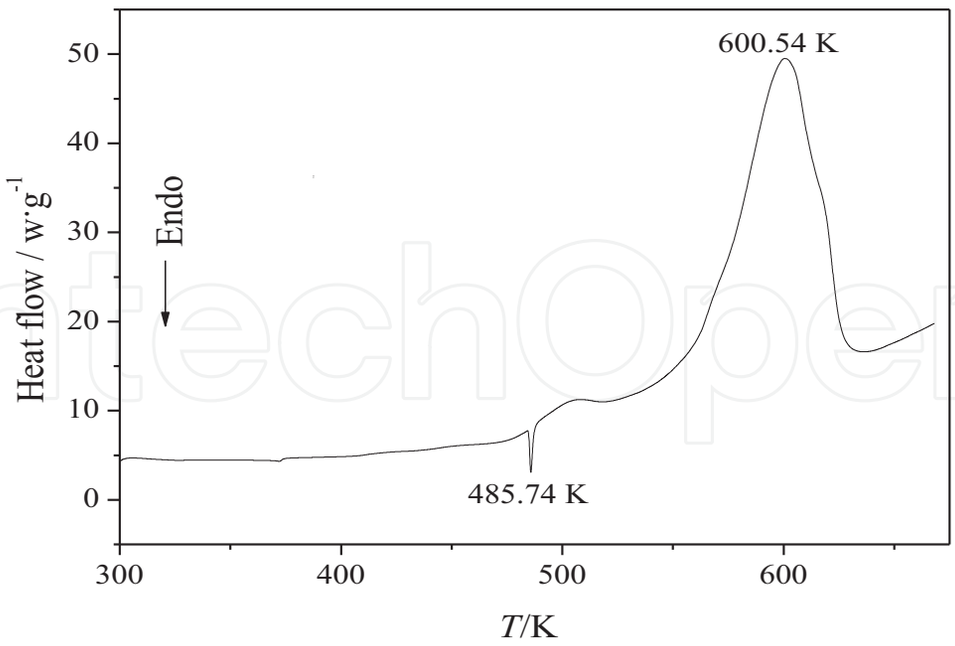

Figure 6. DSC curve of the complex from 300 to 700 K.

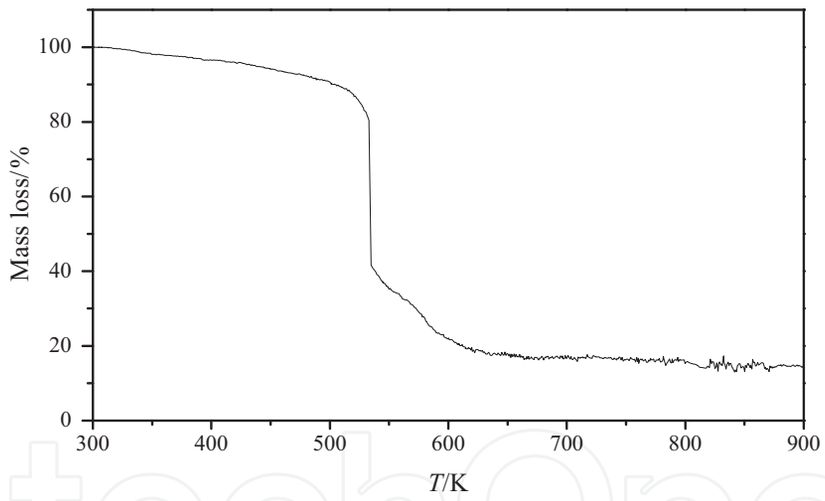

Figure 7. TG curve of the complex from 300 to 900 K.

2.2. Results and discussion

2.2.1. Phase transitions

From the view of phase temperature of the process, Yukawa et al. [43] found a phase transition of the first order and a glass transition of crystalline $(TMA)_2$ **[**$Sm\{Ni(Pro)_2\}_6$**]**$(ClO_4)_4$ at T = (190 ± 1) K and T = (162 ± 2) K. They contributed the phase transition to orientational order/disorder process of perchlorate ions ClO_4^- and the glass transition to a freezing-in phenomenon of the reorientational motion of perchlorate ions ClO_4^-. They discussed that the cooperative interaction between the orientations of the ClO_4^- ions operates through the orientational

and positional shifts of TMA ions, and thus the lattice deformation in the relevant region, associated with the orientational change of the ClO_4^- ions. The position of the ClO_4^- ions itself would shift to form preferable ionic interaction.

It can be seen from **Figure 4** that there are two thermal events in the range 80–350 K on the $C_{p,m}$-T curve. The heat capacity of the sample increases with increasing temperature in a smooth and continuous manner in the temperature range from 80 to 208 K. A little peak occurs at T = 216.98 K on the $C_{p,m}$-T curve, which is consistent with the peak (T_{trs} = 217.30 K) on the DSC curve (**Figure 5**). Such thermal event is deduced to be the phase transition of the complex. The second peak is at 246.08 K, which is also deduced to be the phase transition consistent with the peak (T_{trs} = 245.06 K) on the DSC curve.

It can be proved from **Figure 4** that there are two endothermic processes in the temperature range 100–300 K. One is at 217.30 K, and the other is at 245.06 K, which confirms the results of the heat capacity measurements (216.98 and 246.08 K). The temperature ranges and peak values of the endothermic processes correspond to those of the phase transitions in the $C_{p,m}$-T curve obtained from the heat capacity measurements. It is also verified that there are two phase transitions in the temperature range 100–350 K.

From the view of energy accompanying the process, Yukawa et al. [43] estimated the entropy of the phase transition was to be from 20 to 45 $J{\cdot}K^{-1}{\cdot}mol^{-1}$ in the range. The present work calculated that the molar entropy $\Delta_{trans}S_m$ of the first-phase transition is 27.86 ± 0.08 $J{\cdot}mol^{-1}{\cdot}K^{-1}$, which was in the range of entropy of the phase transition estimated by Yukawa et al.

The combined consideration based on the results of AC (adiabatic calorimetric) and DSC (differential scanning calorimetric) measurements, the values of thermodynamic functions, and the report of former documents leads to a conclusion that the phase transition was interpreted as a freezing-in phenomenon of the reorientational motion of perchlorate ions ClO_4^-. The endothermic process at T = 246.86 K was deduced to be the orientational order/disorder process of ClO_4^- ion [43–46].

2.2.2. Molar heat capacity, molar enthalpies, and entropies

Experimental molar heat capacities, $C_{p,m}$ against temperature T in the range 80–350 K, were listed in **Table 1** and plotted in **Figure 4**. It can be seen from the figure that no phase change or thermal decomposition was found before 206 K and after 258 K.

None-phase transitions process:

Before the solid-solid phase transitions process (from 80 to 208 K):

$$H_T - H_{298.15} = \int_{298.15}^{T} C_{p,m}(s)dT \tag{1}$$

$$S_T - S_{298.15} = \int_{298.15}^{T} [C_{p,m}(s)/T]dT \tag{2}$$

After the solid-solid phase transitions process (from 258 to 350 K):

$$H_{\mathrm{T}} - H_{298.15} = \int_{298.15}^{\mathrm{T_i}} C_{\mathrm{p,m}}(s)dT + \Delta_{trans}H_m + \int_{\mathrm{T}_f}^{\mathrm{T}} C_{\mathrm{p,m}}(s)dT \tag{3}$$

$$S_{\mathrm{T}} - S_{298.15} = \int_{298.15}^{\mathrm{T_i}} [C_{\mathrm{p,m}}(s)/T]dT + \Delta_{trans}S_m + \int_{\mathrm{T}_f}^{\mathrm{T}} [C_{\mathrm{p,m}}(s)/T]dT \tag{4}$$

where $C_{\mathrm{p,m}}$(s) is the molar heat capacity of the solid state, T_{i} is the temperature at which the solid-solid phase transition started, and T_{f} is the temperature at which the solid-solid phase transition ended.

The values of the experimental heat capacities except the phase change regions were fitted. One polynomial Eq. (5) was obtained by least squares fitting using the experimental molar heat capacities ($C_{p,\mathrm{m}}$) and the reduced temperatures (x).

$$C_{p,\,\mathrm{m}}/(\mathrm{J}\cdot\mathrm{K}\cdot\mathrm{mol}^{-1}) = 1838 + 1240x - 136.0x^2 - 806.7x^3 + 376.3\,x^4 + 765.5\,x^5 \tag{5}$$

where $x = [(T/K) - 215]/135$, x is the reduced temperature, and T is the experimental temperature. Correlation coefficient of the least squares fitting, R^2, is 0.9989 (T_i = 80 K and T_{f} =350 K).

Phase transitions process (from 206 to 258 K):

In the solid-solid phase transitions process (from 206 to 258 K), the temperature $T_{\mathrm{trans,}}$ molar enthalpies $\Delta_{\mathrm{trans}}H_{\mathrm{m}}$, and molar entropies $\Delta_{\mathrm{trans}}S_{\mathrm{m}}$ of the first two-phase transitions are determined according to Eqs. (6)–(10) and listed in **Table 3**.

$$\Delta_{\mathrm{trans}}H_{\mathrm{m}} = \sum_{k=1}^{f}[C_{\mathrm{p,m}}(\mathrm{trans})(T_{k+1} - T_k)] \tag{6}$$

$$\Delta_{\mathrm{trans}}S_{\mathrm{m}} = \sum_{k=1}^{f}\left[\frac{C_{\mathrm{p,m}}(\mathrm{trans})}{T_{\mathrm{trans}}}(T_{k+1} - T_k)\right] \tag{7}$$

where $C_{\mathrm{p,m}}$(trans) is the molar heat capacity during the solid-solid phase transitions process:

$$C_{\mathrm{p,\,m}}(\mathrm{trans}) = [C_{p,\,m(k)} + C_{p,\,m_{(k+1)}}]/2 \tag{8}$$

T_{trans} can be seen as follows:

$$T_{\mathrm{trans}} = [(T_k + T_{k+1}]/2 \tag{9}$$

From Eqs. (6) to (9), molar enthalpies, $\Delta_{\mathrm{trans}}H_{\mathrm{m}}$, and molar entropies, $\Delta_{\mathrm{trans}}S_{\mathrm{m}}$, of the two solid-solid phase transition processes from 208 to 228 K and from 228 to 252 K were calculated as follows:

$$\Delta_{\mathrm{trans}}H_{\mathrm{m}} = \sum_{k=1}^{f}[C_{\mathrm{p,m}}(\mathrm{trans},1)(T_{k+1} - T_k)] \tag{10}$$

$$\Delta_{\text{trans}} S_{\text{m}} = \sum_{k=1}^{f} \left[\frac{C_{\text{p,m}}(\text{trans}, 1)}{T_{\text{trans}}} (T_{k+1} - T_k) \right] \tag{11}$$

$$C_{\text{p,m}}(\text{trans}, 1) = C_{\text{p,m}}(\text{trans}) - C_{\text{p,m}}(\text{trans}, 2) \tag{12}$$

where $C_{\text{p,m}}$(trans, 1) is the molar heat capacity caused by solid-solid phase transitions. $C_{\text{p,m}}$(trans) is the total molar heat capacity. $C_{\text{p,m}}$ (trans, 2) is the molar heat capacity induced by temperature change of substance, and its polynomial equation was obtained by least squares analysis using the experimental molar heat capacities in the non-phase transition regions from 80 to 350 K as in Eq. (5).

The molar enthalpy of the first-phase transition was calculated from 208 to 228 K as follows:

$$\Delta_{\text{trans}} H_{\text{m},1} = \sum_{k=1}^{f} [C_{\text{p,m}}(\text{trans}, 1)(T_{k+1} - T_k)] = (3.896 \pm 0.01)\ \text{kJ} \cdot \text{mol}^{-1} \tag{13}$$

$$\Delta_{\text{trans}} S_{\text{m},1} = \sum_{k=1}^{f} \left[\frac{C_{\text{p,m}}(\text{trans}, 1)}{T_{\text{trans}}} (T_{k+1} - T_k) \right] = (17.872 \pm 0.050)\text{J} \cdot \text{mol}^{-1} \cdot \text{K}^{-1} \tag{14}$$

(Standard uncertainty), where T_1 = 208.86 K and T_{f} = 228.55 K.

The molar enthalpy of the second-phase transition was calculated from 228 to 252 K, at 0.1 MPa as follows:

$$\Delta_{\text{trans}} H_{\text{m},2} = \sum_{k=1}^{f} [C_{\text{p,m}}(\text{trans}, 1)(T_{k+1} - T_k)] = (53.763 \pm 0.160)\ \text{kJ} \cdot \text{mol}^{-1} \tag{15}$$

(Standard uncertainty), where T_1 = 228.55 K and T_{f} = 252.57 K. The thermodynamic functions relative to the reference temperature 298.15 K, (H_{T}-$H_{298.15}$), and (S_{T}-$S_{298.15}$) were calculated in the temperature range from 80 to 350 K with an interval of 5 K at pressure 0.1 MPa, and listed in **Table 2**, using the above thermodynamic polynomial Eqs. (1)–(12).

2.2.3. Thermal decomposition properties

It can be seen from **Figure 6** that there are two peaks on the DSC curve from 300 to 700 K. One is a little endothermic peak (T_{trans} = 485.57 K), which was caused by decomposition of amino, and the other is a wide exothermic peak from 530 to 600 K, which was contributed to decomposition of the complex. It was consistent with the results of TG analysis.

The result of TG analysis was showed in **Figure 7**. It can be seen from the TG curve that mass loss of $Eu(Glu)(Im)_5(ClO_4)_3{\cdot}3HClO_4{\cdot}6H_2O$ began at about 298 K and ended at about 900 K. The whole process was divided into three stages. The mechanism of the decomposition was deduced as following:

$$Eu(Glu)(Im)_5(ClO_4)_3 \cdot 3HClO_4 \cdot 6H_2O \xrightarrow[8.10\%(8.0\%)]{300\sim485.88K} Eu(Glu)(Im)_5(ClO_4)_3 \cdot 3HClO_4 \quad (16)$$

$$Eu(Glu)(Im)_5(ClO_4)_3 \cdot 3HClO_4 \xrightarrow[40.90\%(39.43\%)]{531\sim536K} Eu(ClO_4)_3 \cdot 3HClO_4 \quad (17)$$

$$Eu(ClO_4)_3 \cdot 3HClO_4 \xrightarrow[25.7\%(25.45\%)]{536\sim882K} EuO_{3/2}[14.59\%(13.11\%)] \quad (18)$$

The value in the parentheses is theoretical calculation result.

T/K	$C_{p,m}$/J·mol^{-1}·K^{-1}	$(H_T-H_{298.15})$/kJ·mol^{-1}	$(S_T-S_{298.15})$/J·mol^{-1}·K^{-1}
80	879.70	−417.61	−2182.7
85	928.49	−413.09	−2127.0
90	970.11	−408.34	−2072.6
95	1006.0	−403.39	−2019.4
100	1037.4	−398.28	−1967.5
105	1065.6	−393.02	−1916.6
110	1091.5	−387.63	−1866.9
115	1116.0	−382.10	−1818.1
120	1139.9	−376.46	−1770.3
125	1163.8	−370.70	−1723.4
130	1188.3	−364.82	−1677.2
135	1213.9	−358.81	−1631.8
140	1240.8	−352.67	−1587.0
145	1269.4	−346.40	−1542.7
150	1299.9	−339.97	−1498.9
155	1332.3	−333.39	−1455.5
160	1366.7	−326.64	−1412.4
165	1403.1	−319.72	−1369.6
170	1441.4	−312.61	−1327.0
175	1481.5	−305.30	−1284.5
180	1523.2	−297.79	−1242.1
185	1566.3	−290.07	−1199.7
190	1610.6	−282.12	−1157.3
195	1655.9	−273.96	−1114.9
200	1701.8	−265.56	−1072.4
205	1748.2	−256.94	−1029.9
210–250	Phase transitions	\	\
255	2180.7	−100.65	−365.32

T/K	$C_{p,m}$/J·mol^{-1}·K^{-1}	$(H_T\text{-}H_{298.15})$/kJ·mol^{-1}	$(S_T\text{-}S_{298.15})$/J·mol^{-1}·K^{-1}
260	2217.6	−89.657	−322.47
265	2253.2	−78.479	−279.73
270	2287.9	−67.124	−237.11
275	2321.9	−55.598	−194.63
280	2355.6	−43.903	−152.32
285	2389.5	−32.038	−110.16
290	2424.1	−20.002	−68.162
295	2460.2	−7.7892	−26.307
298.15	2484.1	0.0000	0.0000
300	2498.6	4.6103	15.432
305	2540.2	17.210	57.097
310	2586.0	30.028	98.746
315	2637.2	43.088	140.46
320	2695.2	56.422	182.33
325	2761.5	70.067	224.49
330	2837.6	84.069	267.09
335	2925.4	98.481	310.29
340	3027.0	113.37	354.32
345	3144.3	128.80	399.42
350	3279.7	144.87	445.87

Table 2. Thermodynamic functions of the complex from 80 to 350 K at pressure p = 0.1 MPa.

Transition	T_{trans}/K	Δ_{trans} H_m/kJ·mol^{-1}	Δ_{trans} S_m/J·mol^{-1}·K^{-1}
Phase transition I	216.98 ± 0.65	3.896 ± 0.022	17.87 ± 0.05
Phase transition II	246.08 ± 0.74	53.76 ± 0.16	217.9 ± 0.7

Table 3. Temperature, enthalpy, and entropy of the phase transitions of the complex obtained by the heat capacity measurements from 80 to 350 K.

3. Thermodynamic study on rare earth complex of neodymium with glycine: $Nd(Gly)_2Cl_3{\cdot}3H_2O$

3.1. Experiment

3.1.1. Sample preparation and characterization

The complex, $Nd(Gly)_2Cl_3{\cdot}3H_2O$, was synthesized according to the following procedure. Firstly, rare-earth oxide (Nd_2O_3, purity 99.18%) was dissolved in chloride acid to obtain the aqueous solution of the rare-earth chloride. Following that, the aqueous solution was mixed

with glycine in the molar ratio of 1:2 at about pH = 2.5 for 7–8 h. After that, the mixed solution was concentrated in a thermostat bath at 323 K until most of the water was evaporated, and then the concentrated solution was dried in a vacuum desiccator over phosphorus pentoxide for several weeks until lavender crystals appeared.

The actual amount of C, H, and N in the as-prepared sample was confirmed by elemental analysis instrument (model PE-2400 II, USA). The contents of Cl and Nd were determined by the EDTA titration and Mohr method, respectively. The experimental values are: C(10.66%), N (2.97%), H(2.49%), Cl(23.13%) and Nd(31.65%), which are close to the theoretical values of C (10.56%), N(3.08%), H(2.42%), Cl(23.39%) and Nd(31.72%). The sample formula was determined to be $Nd(Gly)_2Cl_3{\cdot}3H_2O$, and the purity obtained from the EDTA titration under the same conditions was found to be 99.78%, which was high enough to meet the requirements of the present calorimetric study. Infrared spectra of the complex $Nd(Gly)_2Cl_3.3H_2O$, $Pr(Gly)_2Cl_3{\cdot}3H_2O$, $Er(Gly)_2Cl_3{\cdot}3H_2O$ and glycine were obtained from KBr pellets at room temperature using an IR spectrophotometer (model AVATAR 370 NICOLET USA).

Infrared spectra of $Nd(Gly)_2Cl_3{\cdot}3H_2O$, $Pr(Gly)_2Cl_3{\cdot}3H_2O$, $Er(Gly)_2Cl_3{\cdot}3H_2O$, and glycine are demonstrated in **Figure 8**. Compared with the IR spectrum of glycine, the νs(carboxyl) band of $Nd(Gly)_2Cl_3{\cdot}3H_2O$ shifted from 1394 cm^{-1} to higher wave numbers (1418 cm^{-1}), which reveals that the carboxyl groups of the ligand have been coordinated to the metal ion. The special absorption of NH_2 shifted from 3105^{-1} to 3420 cm^{-1} (νN-H), from 2604 to 2580 cm^{-1} (νN-H), and from 1500 to 1477 cm^{-1} (υ_{NH_2}) indicates a hydrogen bond formed in the complex. A broad absorption band for νs(hydroxyl) appearing at 3400 cm^{-1} suggests the presence of water molecules in the complex. Meanwhile, it can be observed that main diffraction peaks of Nd

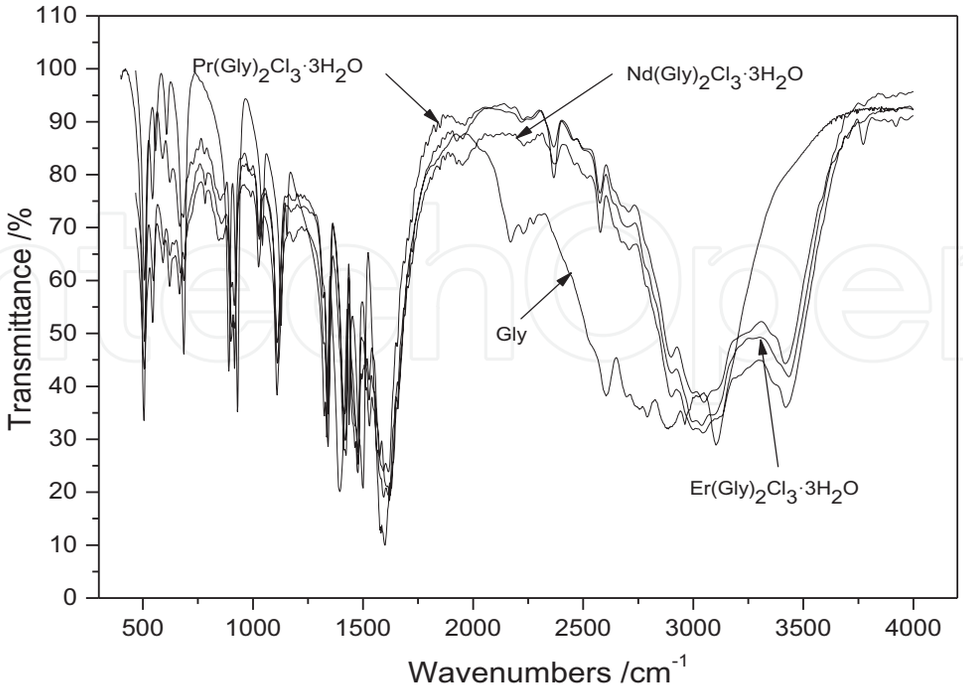

Figure 8. Infrared spectra of the complexes $Nd(Gly)_2Cl_3{\cdot}3H_2O$, $Pr(Gly)_2Cl_3{\cdot}3H_2O$, and $Er(Gly)_2Cl_3{\cdot}3H_2O$.

$(Gly)_2Cl_3{\cdot}3H_2O$ are in good agreement with that of $Pr(Gly)_2Cl_3{\cdot}3H_2O$ and $Er(Gly)_2Cl_3{\cdot}3H_2O$. The above results suggest that the structure of as-synthesized complex is similar to that of $Pr(Gly)_2Cl_3{\cdot}3H_2O$ and $Er(Gly)_2Cl_3{\cdot}3H_2O$.

3.1.2. DSC and TG measurements

Thermal analysis of $Nd(Gly)_2Cl_3{\cdot}3H_2O$ was performed using a differential scanning calorimeter (DSC-141, SETARAM, France) and a thermogravimetric analyzer (model DT-20B, Shimadzu, Japan). The DSC measurement was carried out with a heating rate of 10 K^{-1} min^{-1} under high-purity nitrogen with a flow rate of 50 mL^{-1} min^{-1}. The mass of the sample used in the experiment was 3.36 mg. The calibrations for the temperature and heat flux of the calorimeter were performed prior to the experiment. The temperature scale was calibrated by measuring the melting points of Hg, In, Sn, Pb, and Zn at different heating rates, and the heat flux was calibrated using the Joule effect. Measurement of the melting temperature and the enthalpy of fusion of benzoic acid (NIST, SRM 39i) were carried out in this laboratory to check the accuracy of the instrument. The TG measurement of the complex was conducted at a heating rate of 10 K^{-1} min^{-1} under high-purity nitrogen with a flow rate of 120 $mL{\cdot}min^{-1.}$ The mass of the sample used in the experiment was 9.47 mg. The reference crucible was filled with α-Al_2O_3. The TG-DTG equipment was calibrated by the thermal analysis of the SRM, $CaC_2O_4{\cdot}H_2O$(s).

3.1.3. Dissolution enthalpy measurements

3.1.3.1. Isoperibol solution reaction calorimeter

The Isoperibol solution reaction calorimeter (SRC-100) used for this study was constructed in our thermochemistry laboratory and has been used for measuring enthalpies of solid-liquid, liquid-liquid dissolution reactions enthalpies of the reactant, and the product to obtain the formation enthalpies of the complex. The principle and structure of the instrument were described elsewhere [47]. The schematic diagram of the calorimeter is shown in **Figure 9**. The calorimeter mainly consisted of a water thermostat, a pyrex-glass Dewar with volume of 100 mL, a glass sample cell with volume of 2 mL, a heater for calibration and equilibration purposes, a glass-sheathed thermistor probe, an amplifier, a circuit used as an A/D converter, and a personal computer for data acquisition and processing. The Dewar vessel, equipped with a twin-blade stirrer, served as a mixing chamber, was submerged in the water thermostat. The precisions of controlling and measuring the temperature of the calorimeter are ±0.001 and ±0.0001 K, respectively. The measurements of solution-reaction enthalpy of samples were conducted under atmospheric pressure. The calorimeter was tested by measuring the dissolution enthalpies of the KCl (calorimetric primary standard) in water at 298.15 K. The mean dissolution enthalpies obtained from five experiments are 17515 ± 12 $J{\cdot}mol^{-1}$, which are in conformity with the reported data (17536 ± 9 $J{\cdot}mol^{-1}$) [48].

3.1.3.2. Dissolution and formation enthalpy measurements

The dissolution enthalpies of reactants and the products, and standard molar enthalpy of formation of $Nd(Gly)_2Cl_3{\cdot}3H_2O$ were determined through the proposed Hess thermochemical cycle, which is demonstrated in **Figure 10**. The dissolution enthalpy of H_2O (l), $\Delta_d H$, as one of

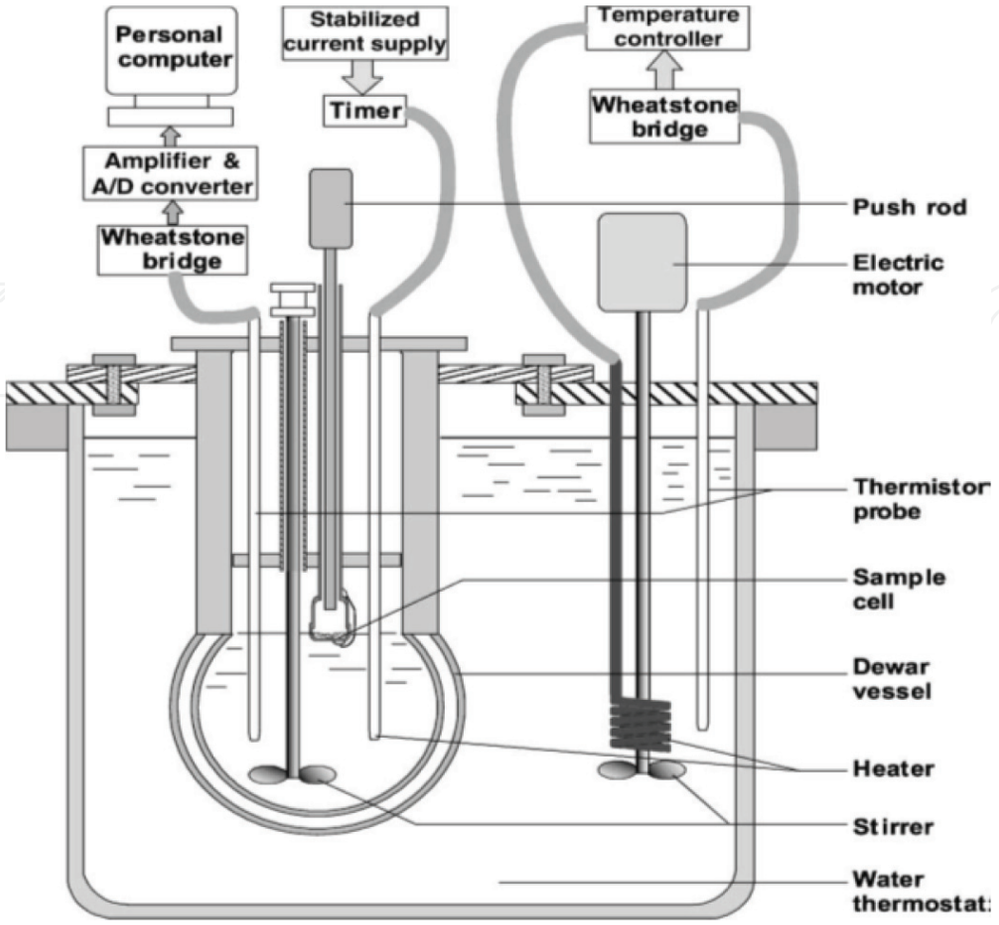

Figure 9. The schematic diagram of isoperibol solution-reaction calorimeter.

the products in above cycle under the same condition was within the range of experimental error and may be omitted because the amount of H_2O (l) was very small according to the stoichiometric number of H_2O (l) in above cycle.

As illustrated in **Figure 10**, the molar enthalpy of formation of $Nd(Gly)_2Cl_3{\cdot}3H_2O(s)$ is given as:

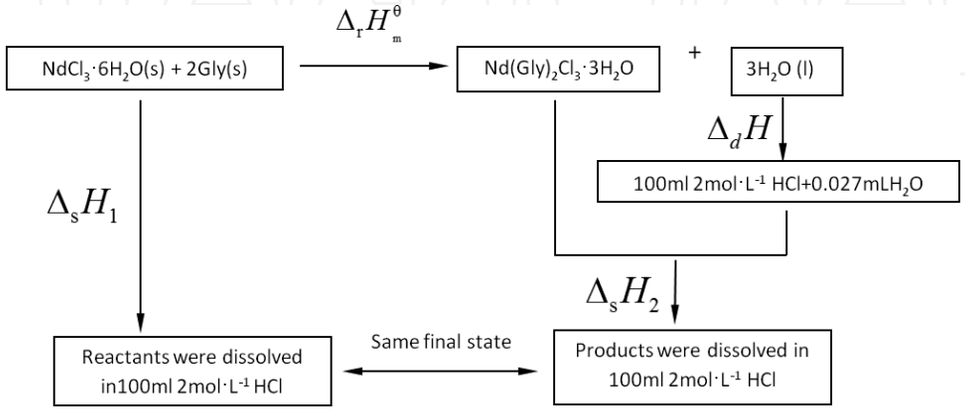

Figure 10. Hess thermochemical cycle.

$$\Delta_r H^\theta{}_m = \Delta_f H^\theta{}_m[\mathrm{Nd(Gly)_2Cl_3 \cdot 3H_2O, s}] + 3\Delta_f H^\theta{}_m(\mathrm{H_2O, l}) + \Delta_f H^\theta{}_m(\mathrm{NdCl_3 \cdot 6H_2O, s}) \\ +2\Delta_f H^\theta{}_m(\mathrm{Gly, s}) = \Delta s H_1 - \Delta s H_2 - \Delta_d H \approx \Delta s H_1 \Delta s H_2 \quad (19)$$

where $\Delta_f H^\theta{}_m[\mathrm{Nd(Gly)_2Cl_3 \cdot 3H_2O,s}]$, $\Delta_f H^\theta{}_m(\mathrm{NdCl_3 \cdot 6H_2O,s})$, and $\Delta_f H^\theta{}_m(\mathrm{Gly,s})$ are the molar enthalpy of formation of the corresponding compounds. $\Delta_f H^\theta{}_m$ $[\mathrm{Nd(Gly)_2Cl_3 \cdot 3H_2O,s}]$ could be calculated from the following equation:

$$\Delta_f H^\theta{}_m[\mathrm{Nd(Gly)_2Cl_3 \cdot 3H_2O, s}] = \Delta s H_1 - \Delta s H_2 + \Delta_f H^\theta{}_m(\mathrm{NdCl_3 \cdot 6H_2O, s}) \\ +2\Delta_f H^\theta{}_m(\mathrm{Gly, s}) - 3\Delta_f H^\theta{}_m[\mathrm{H_2O, l}] \quad (20)$$

The mixture of $\mathrm{NdCl_3 \cdot 6H_2O(s)}$ and Gly(s) at mole ratio of $n(\mathrm{NdCl_3 \cdot 6H_2O})$:$n$(Gly) = 1:2 was dissolved in 100 mL of 2 mol·L^{-1} HCl at 298.15 K. The final solution obtained was named as Solution A. Dissolution enthalpy of 1 mol $\mathrm{Nd(Gly)_2Cl_3 \cdot 3H_2O}$ (s) in 100 mL of 2 mol·L^{-1} hydrochloric acid was determined under the same condition as above. The final solution obtained was named as Solution A′. Finally, UV–vis spectroscopy and the data of the refrangibility were applied to confirm whether Solution A was in the same thermodynamic state as that of Solution A′. These results mentioned above indicated that chemical components and physical-chemistry properties of Solution A were consistent with those of Solution A′. In this chapter, UV–vis spectrum and the data of the refrangibility of Solution A obtained agreed with those of Solution A′. These results demonstrated that the designed thermochemical cycle is reasonable and reliable, hence can be used to calculate the standard molar enthalpy of formation of $\mathrm{Nd(Gly)_2Cl_3 \cdot 3H_2O(s)}$.

3.2. Results and discussion

3.2.1. Thermal analysis

The thermal analysis results of $\mathrm{Nd(Gly)_2Cl_3 \cdot 3H_2O}$ are shown in **Figures 11** and **12**, respectively. The DSC curve (**Figure 11**) reveals that the two endothermic peaks appear at 146.68 and 282.21°C, which are in agreement with those obtained from the TG-DTG (thermogravimetric-differential thermogravimetric) experiments at 147.5 and 283.0°C.

The mass loss of $\mathrm{Nd(Gly)_2Cl_3 \cdot 3H_2O}$ was mainly divided to two steps. Based on the TG curve and the structure of $\mathrm{Nd(Gly)_2Cl_3 \cdot 3H_2O}$, the conclusion can be drawn that from 59 to 188°C the three coordinating water molecules break away from the complex. The experimental mass loss (%) of the first step was found to be 8.9%. The result is consistent with the theoretical mass loss, 11.9%, of the three water molecules. The second step of the mass loss from 262 to 904°C should be due to the glycine being separated from the Nd^{3+} cations, and the residue of the TG experiment should be $NdCl_3$ and Nd. The experimental mass loss (%) of the decomposition is 52.8%, which is in accord with the theoretical mass loss, 48.6%. The possible mechanism of the thermal decompositions was deduced as

$$3\mathrm{Nd(Gly)_2Cl_3 \cdot 3H_2O} \xrightarrow[8.9\%\ (11.9\%)]{59-188^\circ\mathrm{C}} 3\mathrm{Nd(Gly)_2Cl_3} \\ \xrightarrow[52.8\%\ (48.6\%)]{262-904^\circ\mathrm{C}} \mathrm{NdCl_3} + 2\mathrm{Nd}$$

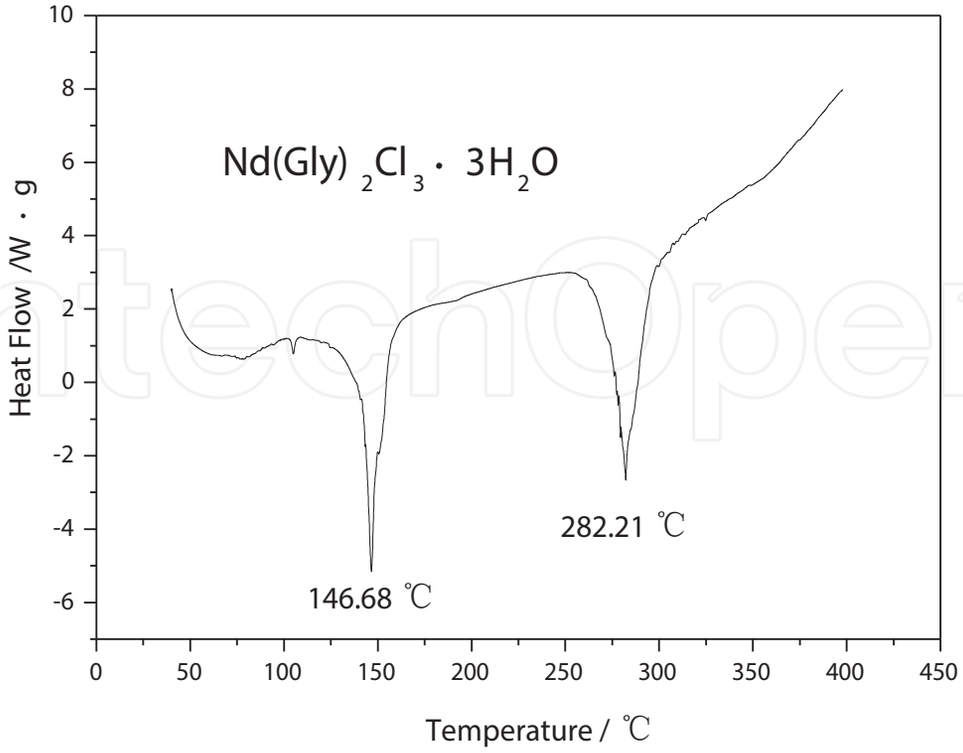

Figure 11. DSC curve of the complex $Nd(Gly)_2Cl_3{\cdot}3H_2O$.

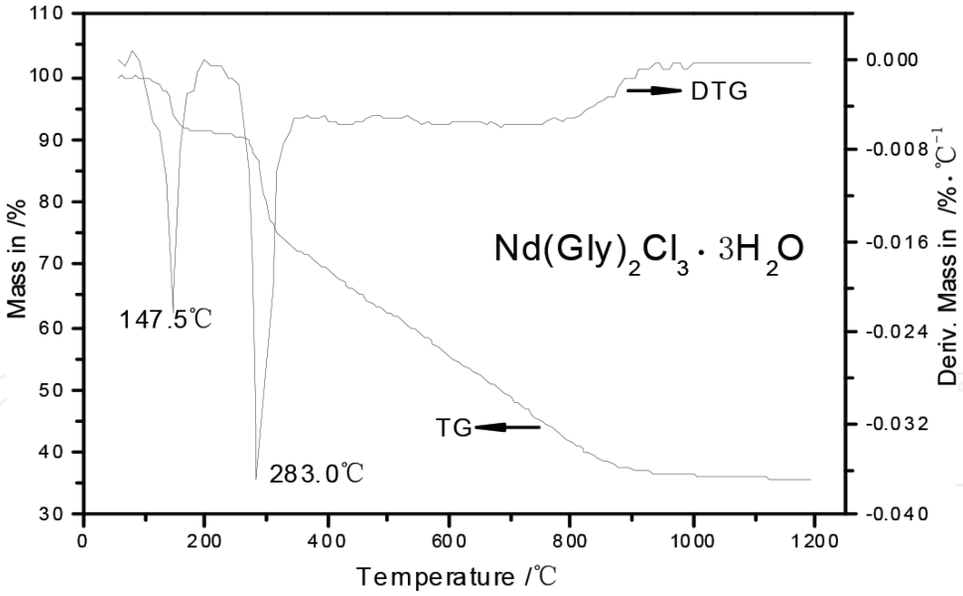

Figure 12. TG-DTG curves of the complex $Nd(Gly)_2Cl_3{\cdot}3H_2O$.

3.2.2. The standard molar enthalpy of formation of the complex $Nd(Gly)_2Cl_3{\cdot}3H_2O$

The experimental values of the dissolution enthalpies of the mixture prepared at the mole ratio of the reactants were measured. Dissolution enthalpies $\Delta_s H_1$ and $\Delta_s H_2$ were determined by the dissolution process tested. The experiment was repeated five times in the same condition, and

No.	1	2	3	4	5	Mean value
$\Delta_s H_1$/kJ·mol^{-1}	4.5298	−4.7254	−4.3564	−4.4486	−4.2986	−4.4718
$\Delta_s H_2$/kJ·mol^{-1}	10.3709	10.3722	10.3699	10.3678	10.3731	10.3707

Table 4. The determination results of the ΔsH_1 and ΔsH_2 at 298.15 K.

the results were listed in **Table 4**. The enthalpy change $\Delta_r H^\theta{}_m$ could be calculated in accordance with expression (19) as follows:

$$\Delta_r H^\theta{}_m = \Delta sH_1 - \Delta sH_2 = -4.4718 - 10.3707 = (-14.8425 \pm 0.1512)\text{kJ} \cdot \text{mol}^{-1}$$

The experimental values of the dissolution enthalpies of the reactants and products in the thermochemical cycle are combined with the following auxiliary thermodynamic data:

$$\Delta_f H^\theta{}_m(\text{NdCl}_3 \cdot 6\text{H}_2\text{O}, \text{s}) = -2867.5 \text{ kJ} \cdot \text{mol}^{-1} \text{ [49]}$$

$$\Delta_f H^\theta{}_m(\text{H}_2\text{O}, \text{l}) = -285.8 \text{ kJ} \cdot \text{mol}^{-1} \text{ [49]}$$

$$\Delta_f H^\theta{}_m(\text{Gly}, \text{s}) = -528.5 \text{ kJ} \cdot \text{mol}^{-1} \text{ [50]}$$

According to the expression (20), the standard molar enthalpy of formation of the complex Nd (Gly) $^2Cl^3{\cdot}3H^2O$ (s) at 298.15 K can be calculated as follows:

$$\Delta_f H^\theta{}_m[\text{Nd(Gly)}_2\text{Cl}_3 \cdot 3\text{H}_2\text{O}, \text{s}] = (-3081.3 \pm 1.08)\text{kJ} \cdot \text{mol}^{-1}$$

4. Microcalorimetric study on biological effect of rare-earth complex with amino acid: $La(Glu)(Im)_6(ClO_4)_3{\cdot}4HClO_4{\cdot}4H_2O$

4.1. Experiment

4.1.1. Synthesis and characterization of the complex

The complex, $La(Glu)(Im)_6(ClO_4)_3{\cdot}4HClO_4{\cdot}4H_2O$, was synthesized in water solution. All the starting materials were analytical reagents from the Beijing Chemical Reagent Co. Rare-earth oxide (La_2O_3) was dissolved in an excess amount of perchloric acid, and the concentration of the solution was determined by EDTA（ethylene diamine tetraacetic acid) titrimetric analysis. Then solid glutamic acid was added to the solution of La^{3+} in molar ratio of La^{3+}:Glu = 1:1. After the pH value of the reaction mixture was carefully adjusted to 6.0 by adding 0.1 mol·L^{-1} NaOH slowly, imidazole was added as the same molar as glutamic acid. The reaction was performed at 60°C in water bath for 5 h. Then the solution was condensed at 80°C for 5 h and put into desiccator in the fridge at −4°C. The crystal was obtained after about one month.

An elemental analysis apparatus (Model PE-2400 II, USA) was used to measure the ratio of C, H, and N in the complex. Content of La % was determined by EDTA titration. The experimental values are: La, (9.423%), C (18.363%), N (12.964%) and H (2.736%), which are close to the theoretical values, La (9.057%), C (18.883%), N (12.452%) and H (2.805%). The sample formula

was determined to be $La(Glu)(Im)_6(ClO_4)_3{\cdot}4HClO_4{\cdot}4H_2O$, and the purity obtained from the EDTA titration under the same conditions was found to be 99.79%.

IR spectra were obtained using KBr pellets with a Tensor 27 (Bruker) spectrometer. It can be seen from the IR spectra of the complex that the symmetrical resonance frequencies, $\nu_{s\ (COO\text{-})}$, shifted from 1431 to 1413 cm^{-1}, which suggests that the carboxyl group of Glu has coordinated to the metal ions.

4.1.2. The Escherichia coli *(*E. coli*) DH5α*

The *E. coli* DH5α was provided by Biomass Conversion Technology Group, Dalian Institute of Chemical Physics, CAS, Dalian 116023, PR China. The strain of *E. coli* DH5α was stored in 10% glycerol solution at −20°C.

The *E. coli* DH5α used in the present research was prepared as follows. A single colony of *E. coli* DH5α from LB(Luria-Bertani) plates was inoculated into a 10 mL LB culture medium and cultivated at 37°C in a rotary shaker (220 rpm) for 12 h under aerobic condition. Then, 200 μL of the above suspension was inoculated into 10 mL LB culture medium at 37°C in a rotary shaker (220 rpm) for 2.5 h once again. The value of optical density (OD) of the *E. coli* DH5α suspension was measured to be about 0.6 by spectrophotometry at λ = 600 nm. Per 200 mL of LB culture medium contained 2 g tryptone, 1 g yeast extract powder, 2 g and NaCl (pH 7.0–7.2). It was sterilized in high-pressure steam at 120°C for 20 min before experiment.

4.1.3. Microcalorimeter

Thermal Analysis Microcalorimeter (TAM) Air is a type of eight-channel twin isothermal microcalorimeters that originally was developed for the study of the hydration process of cement and concrete. TAM represents an ultra-sensitive heat flow measurement which is complementary to TA instruments differential scanning calorimeters (DSC). "Air" means the thermostat type. However, the high sensitivity and excellent long-term stability make TAM Air useful also for other applications such as stability testing of energetic materials, determining the shelf life of food and monitoring biological processes [51].

A TAM Air Isothermal Microcalorimeter (see **Figure 13**) manufactured by Thermometric AB Company of Sweden (incorporated by TA Instruments in 2006) was used to measure the power-time curves of the metabolism of *E. coli* DH5α at 37°C. The main structure of the instrument is eight channels, each of which consists of aluminum heat sink, vessel holder, and thermocouple plate, and each two of them are twin. Glass reaction vessel of 20 mL was used in each channel. The working temperature in the instrument was 5–60°C controlled by air thermostat. The deviation of the controlled temperature is within ±0.02°C. A computer was employed to record the voltage-time signals continuously which were converted to power-time signals through calibration. Thermal power detection limit was stated to be ± 2 μW. The development and theory of many kinds of multi-channel isothermal microcalorimeters have been studied by Wadsö [52, 53].

The ampoule method was used for the microcalorimetric measurement in this work. Luria-Bertani (LB) culture medium (10 mL) containing object compound with different concentrations

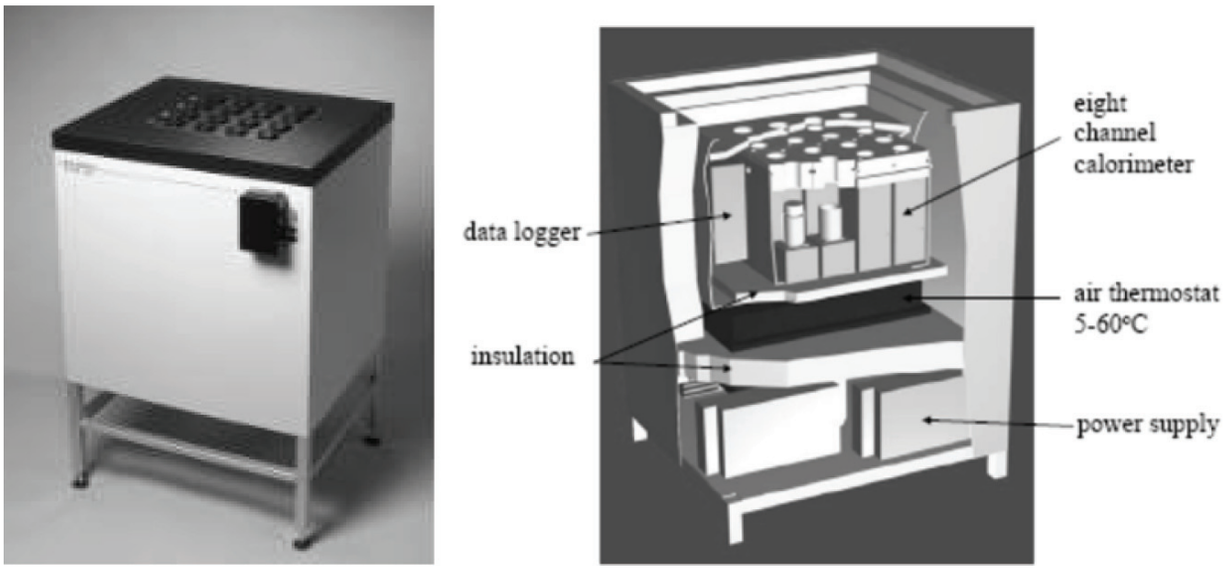

Figure 13. Practicality and cutaway views of TAM Air 8-channel isothermal calorimeter.

was put into eight sample ampoules, which had been cleaned and sterilized. Then, the *E. coli* DH5α suspension was inoculated into the above eight ampoules. At last, the ampoules were sealed with ampulla cap by ampoule filler. The working temperatures of the calorimeter were set and controlled at 37°C. The power-time signals were recorded at intervals of 1 min.

The ampoule method was used for the microcalorimetric measurement in this work. LB culture medium (10 mL) containing object compound with different concentrations was put into eight sample ampoules, which had been cleaned and sterilized. Then, the *E. coli* DH5α suspension was inoculated into the above eight ampoules. At last the ampoules were sealed with ampulla cap by ampoule filler. The working temperatures of the calorimeter were set and controlled at 37°C. The power-time signals were recorded at intervals of 1 min.

4.2. Results and discussion

4.2.1. Thermokinetics

In the log phase of growth, the growth of *E. coli* DH5α cells is exponential [54]. It can be expressed as follows:

$$n_t = n_0 \exp(kt) \tag{21}$$

Where t is the incubation time, n_t is the cell number at time t, n_0 is the initial cell number, and k is the constant of cell growth rate. If the power output of each cell is denoted as Pw, then

$$n_t P\mathrm{w} = n_0 P\mathrm{w} \exp(kt) \tag{22}$$

We define P_0 as the initiative power output and P_t as the power output at time t, then Eq. (2) can be rewritten as follows:

$$P_t = P_0 \exp(kt) \tag{23}$$

or

$$\ln P_t = \ln P_0 + kt \tag{24}$$

For thermokinetic parameters, inhibitory ratio (I) is defined as:

$$I = [(k_0 - k_c)/k_0]/100\% \tag{25}$$

Where k_0 is the rate constant of the control, and k_c is the rate constant of *E. coli* DH5α growth inhibited by the complex with a concentration of C.

4.2.2. Thermokinetic parameters

Figures 14 and **15** show the growth power-time curves of *E. coli* DH5α under various concentrations (0–5.0 μg·m mL^{-1}) of the complex at 37°C. It can be seen from the figures that growth curve of *E. coli* DH5α can be divided into four typical phases, which are lag phase, log phase, stationary phase, and decline phase. The thermokinetic parameters of growth, growth rate constants (k/10^{-3}·min^{-1}), the maximum heat power (P_m/μW), and the time of the maximum heat power (t_m/min) are derived from the curves by using Eqs. (1)–(5), and the results are listed in **Tables 5** and **6**.

The relationships among the concentration (C), the rate constant (k), and the maximum heat power (P_m) were plotted in **Figure 16** at different concentrations (0, 0.1, 0.5, and 1.0 μg·mL^{-1}) based on the data of **Table 5**. It can be seen from **Figure 16** that the rate constant (k) and the maximum heat power (P_m) were both increasing with the increase of the concentration from

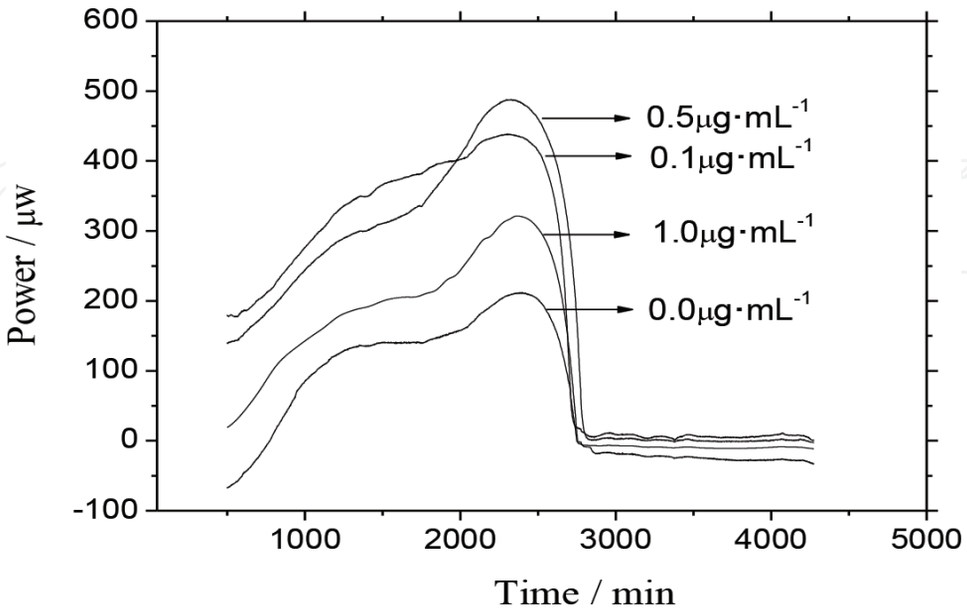

Figure 14. Growth curves of *E. coli* DH5α at different concentrations (0, 0.1, 0.5, and 1.0 μg·mL^{-1}) of the complex at 37°C.

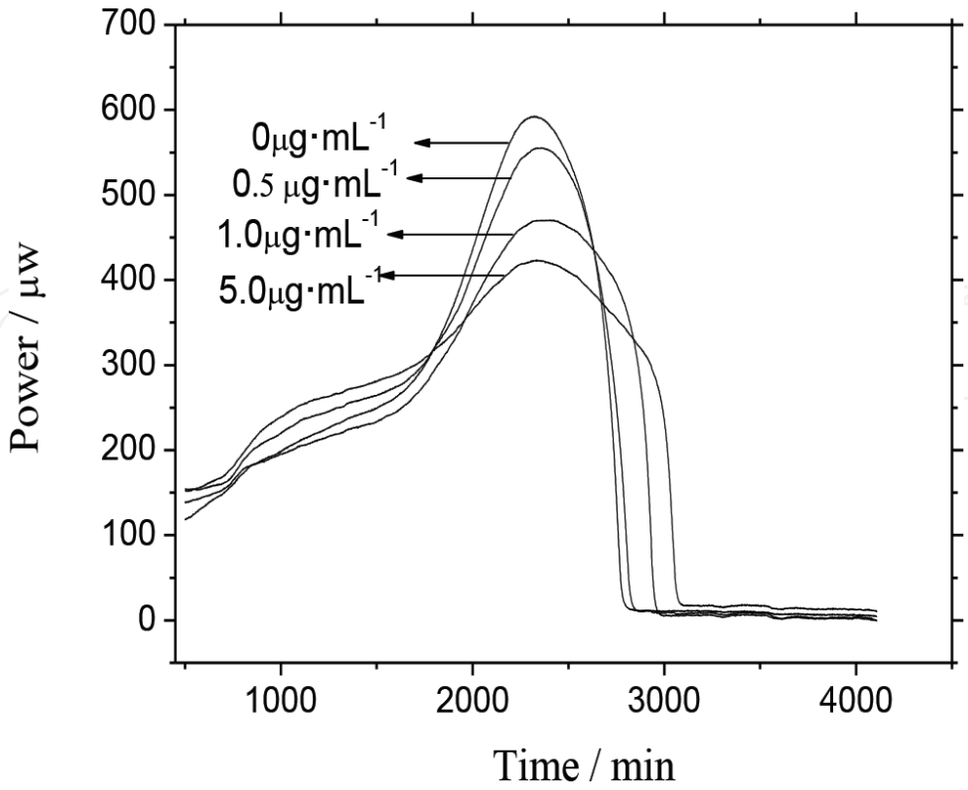

Figure 15. Growth curves of *E. coli* DH5α at different concentrations (0, 0.5, 1.0, and 5.0 μg·mL^{-1}) of the complex at 37°C.

C/μg·mL^{-1}	k/10^{-3}·min^{-1}	R	P_m/μW	t_m/min	I%
0	0.2	0.9992	211.9	2390	0
0.1	0.25	0.9967	438.2	2297	13.3
0.5	0.3	0.9989	488.0	2328	20.0
1.0	0.08	0.9981	379.6	2391	53.3

Table 5. Thermodynamic parameters of growth of *E. coli* DH5α at different concentrations of the complex.

C/μg·mL^{-1}	k/10^{-3} min^{-1}	R	P_m/μW	t_m/min	I%
0	1.5	0.9993	592.3	2308	0
0.5	1.3	0.9961	555.4	2365	25
1.0	1.2	0.9985	470.5	2422	50
5.0	0.7	0.9981	423.8	2332	80

Table 6. Thermodynamic parameters of growth of *E. coli* DH5α at different concentrations of the complex.

0 to 0.5 μg mL^{-1}, which indicated that the complex could speed up the growth of *E. coli* DH5α. When the concentration (C) reached 0.5 μg mL^{-1}, the value of rate constant (k) showed a highest value. It demonstrated that the complex could promote clearly the growth of *E. coli*

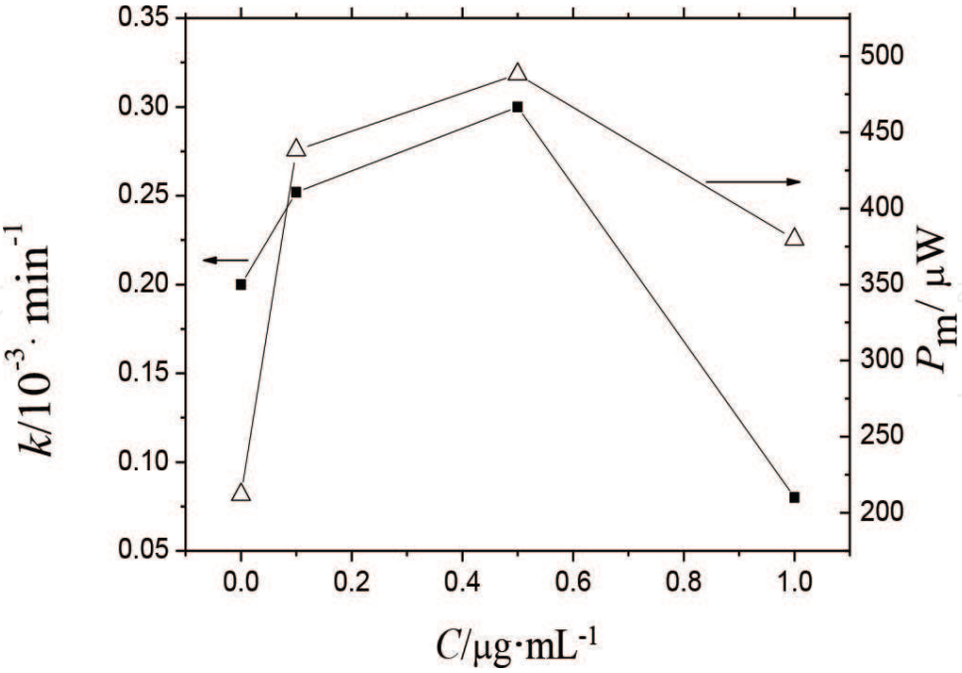

Figure 16. *K-c* curves of *E. coli* DH5α at different concentrations (0, 0.1, 0.5, and 1.0 μg mL^{-1}) of the complex at 37°C.

DH5α at this time. At the concentration (*C*) from 0.5 to 1.0 μg mL^{-1}, the line decreased, which was consistent with **Figure 17**.

Figure 17 was plotted from the data of **Table 6**, when the concentration (*C*) was from 0.5 to 5.0 μg mL^{-1}. It showed that the rate constant (*k*) and the maximum heat power (P_m) were both decreasing with the increase of the concentration (*C*), which indicated that the complex inhibited the growth of *E. coli* DH5α at this range of concentrations (*C*). When the concentration reached 5.0 μg mL^{-1}, *E. coli* DH5α almost could not grow.

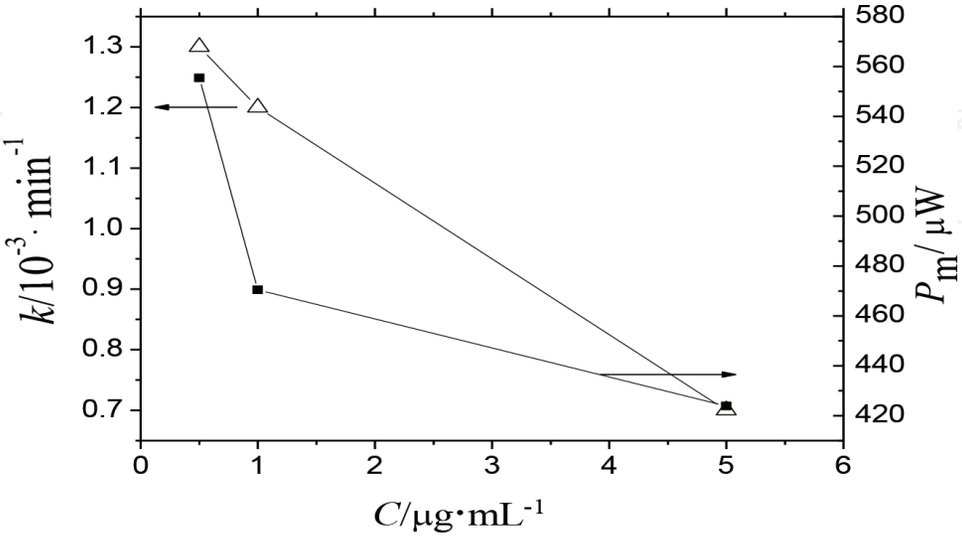

Figure 17. *K-c* curves of *E. coli* DH5α at different concentrations (0, 0.5, 1.0, and 5.0 μg·mL^{-1}) of the complex at 37°C.

5. Conclusions

In this chapter, the following three rare-earth complexes with amino acids were synthesized and characterized by element analysis, infrared（IR） spectrum, and x-ray diffraction (XRD) analysis. The thermodynamic property studies on these complexes were performed. For the first rare-earth complex, $Eu(Glu)(Im)_5(ClO_4)_3{\cdot}3HClO_4{\cdot}6H_2O$, the low-temperature molar heat capacity was measured by adiabatic calorimetry. Two thermal abnormalities interpreted as phase transitions were discovered at 216.18 and 246.86 K by the AC technique, and proved by DSC. The thermodynamic functions $[H_T\text{-}H_{298.15}]$ and $[S_T\text{-}S_{298.15}]$ were derived in the temperature range from 80 to 320 K. The mechanism of thermal decomposition was deduced in terms of the results of TG. For the second rare-earth complex, $Nd(Gly)_2Cl_3{\cdot}3H_2O$, the standard molar enthalpy of formation was determined to be (-3081.3 ± 1.08) kJ·mol^{-1} by an isoperibol solution-reaction calorimeter in terms of a designed thermochemical cycle. For the third rare-earth complex, $Eu(Glu)(Im)_5(ClO_4)_3{\cdot}3HClO_4{\cdot}6H_2O$, the microcalorimetry was used to investigate the interaction between the complex and the *Escherichia coli* DH5α to elucidate the biological effects of the complex. The thermokinetic parameters of growth of the *E. coli* DH5α were obtained. The results show that the complex has a stimulatory effect on the growth of *E. coli* DH5α below the concentration 0.5 μg mL^{-1}, and the complex could inhibit its growth in the concentration range between 0.5 and 5.0 μg mL^{-1}.

Acknowledgements

This work was financially supported by the National Natural Science Foundation of China under the grant NSFC No. 20373072 and 21473198. Parts of this chapter are reproduced from authors' recent conference publication, work, etc. [33, 36].

Author details

Zhi Cheng Tan[1]*, Quan Shi[1], Xue Chuan Lv[2] and Bei Ping Liu[3]

*Address all correspondence to: tzc@dicp.ac.cn

1 Thermochemistry Laboratory, Dalian Institute of Chemical Physics, Chinese Academy of Science, Dalian, China

2 School of Chemistry and Material Science, College of Chemistry Chemical Engineering and Environmental Engineering, Liaoning Shihua University, Fushun, China

3 College of Chemistry and Materials Engineering, Hunan University of Arts and Science, Hunan, China

References

[1] Tan ZC, Zhang ZY, Yin JZ, Jiang BG, Sun TS. Low-temperature heat capacities and thermodynamic properties of rare-earth triisothiocyanate hydrates, $RE(NCS)_3$. nH_2O. Chinese Science Bulletin. 1991;**36**(13):1086–1090

[2] Tan ZC, Takasuke M, Hiroshi S, Zhang ZY, Yin JZ, Jiang BG, et al. Low temperature heat capacities and thermodynamic properties of rare earth triisothiocyanate hydrate. 1. La $(NCS)_3$ ·$7H_2O$ and $Ce(NCS)_3$ ·$7H_2O$. Science in China Series B-Chemistry. 1992;**35**(4):1391–1403

[3] Tan ZC, Takasuke M, Hiroshi S, Zhang ZY, Yin JZ, Jiang BG, et al. Low temperature heat capacities and thermodynamic properties of rare earth triisothiocyanate hydrates. 2. Pr $(NCS)_3$ $7H_2O$ and $Nd(NCS)_3$ $7H_2O$. Science in China Series B-Chemistry. 1996;**39**(3):276–284

[4] Tan ZC, Takasuke M, Hiroshi S, Zhang ZY, Yin JZ, Jiang BG, et al. Low-temperature heat capacities and thermodynamic properties of rare-earth triisothiocyanate hydrates 3. Sm $(NCS)_3$·$6H_2O$, $Gd(NCS)_3$·$6H_2O$, $Yb(NCS)_3$ ·$6H_2O$ and $Y(NCS)_3$·$6H_2O$. Science in China, Series B-Chemistry. 1997;**40**(2):165–176

[5] Anghileri LJ. On the antitumor activity of gallium and lanthanides. Arzneim-Forsch. 1975;**25**:793–795

[6] McCarthy GJ. Rare Earths in Modern Science and Technology. Vol. 2. Plenum Press; New York, 1980. pp. 25–105

[7] Sudhindra NM, Joshi GK, Bhutra MP. Syntheses and absorption spectral studies of Praseodymium (II) and Neodymium (II) complexes with amino acids. Indian Journal of Chemistry. 1982;**21A**:275–278

[8] Glowiak T, Legendziewicz J, Huskowska E, Gawryszewska P. Ligand chirality effect on the structure and its spectroscopic consequences in $[Ln_2(Ala)_4(H_2O)_8](ClO_4)_6$. Polyhedron. 1996;**15**:2939–2947

[9] Zhang H, Feng J, Zhu WF. Rare-earth element distribution charcteriatics of biological chains in rare-earth element-high background regions and their implications. Biological Trace Element Research. 2000;**73**:19–27

[10] Xu H, Chen L. Study on the complex site of L-tyrosine with rare-earth element Eu^{3+}. Spectrochimica Acta Part A. 2003;**59**:657–662

[11] Li GT, Zhang DS, Li L, Tan ZC, Wu XM, Meng SH. Low-temperature heat capacity and thermochemical study of $Re_2(Pro)_6(H_2O)_4$ $(ClO4)_6$ (Re = Nd, Gd; Pro = proline) crystals. Thermochimica Acta. 2001;**375**(1–2):125–130

[12] Wu XM, Liu Y, Li L, Liu P, Tan ZC, Qu SS. Low-temperature heat capacity and standard enthalpy of formation of samarium glycine perchlorate complex $Sm_2(Gly)_6(H_2O)_4$ $(ClO4)_6$. $5H_2O$. Acta Chimica Sinica. 2001;**59**(9):1396–1400

[13] Liu BP, Tan ZC, Nan ZD, Liu P, Sun LX, Xu F. Calorimetric study and thermal analysis of $[Ho_2(Ala)_4(H_2O)_8]Cl_6$ and $[ErY(Ala)_4(H_2O)_8]$ $(ClO4)_6$. Acta Physico-Chimica Sinica. 2002;**18**(6):481–485

[14] Liu BP, Zhao XS, Li L, Sun LX, Tan ZC. Low-temperature heat capacity and thermochemical study of crystalline $[Y_2(Ala)_4(H_2O)_8]$ $(ClO_4)_6$ (Ala=$CH_3CH(NH_3^+)(COO^-)$). Thermochimica Acta. 2002;**389**(1-2):59–64

[15] Liu BP, Tan ZC, Zhang DS, Nan ZD, Sun LX, Xu F, et al. Low-temperature heat capacity and thermodynamic properties of crystalline $[Re_2(Ala)_4$ $(H_2O)_8]$ $(ClO4)_6$ (Re = Eu, Er; Ala = alanine). Thermochimica Acta. 2002;**390**(1–2):31–37

[16] Lan XZ, Tan ZC, Liu BP, Nan ZD, Sun LX, Xu F. Low-temperature heat capacity and thermal decomposition of crystalline $[Ho(Thr)(H_2O)_5]Cl_3$. Chinese Journal of Chemistry. 2003;**21**(8):1043–1046

[17] Lan XZ, Tan ZC, Liu BP, Nan ZD, Sun LX, Xu F. Low-temperature heat capacity and thermodynamic properties of $[Re_2(Ile)_4(H_2O)_8$ $(ClO_4)_6$ (Re = Nd, Er, Ile = isoleucine). Thermochimica Acta. 2003;**402**(1-2):183–191

[18] Liu BP, Tan ZC, Lan XZ, Yu HG, Zhang DS, Sun LX. Calorimetric study and thermal analysis of $[Gd_{4/3}Y_{2/3}(Gly)_6(H_2O)_4]\cdot(ClO_4)_6\cdot 5H_2O$ and $[ErY(Gly)_6(H_2O)_4]$ $(ClO_4)_6\cdot 5H_2O$ (Gly = glycin). Thermochimica Acta. 2003;**401**(2):233–238

[19] Liu BP, Tan ZC, Lu JL, Lan XZ, Sun LX, Xu F, et al. Low-temperature heat capacity and thermodynamic properties of crystalline $RE(Gly)_3(H_2O)_2$ $Cl_3\cdot 2(H_2O)$ (RE = Pr, Nd, Gly = Glycine). Thermochimica Acta. 2003;**397**(1-2):67–73

[20] Liu BP, Tan ZC, Nan ZD, Liu P, Sun LX, Xu F, et al. Calorimetric study and thermal analysis of $[ErY(Ala)_4(H_2O)_8](ClO_4)_6$ (Ala=alanine). Journal of Thermal Analysis and Calorimetry. 2003;**71**(2):623–628

[21] Liu BP, Tan ZC, Yu HG, Lan XZ, Zhang DS, Liu P, et al. Thermodynamic properties of $[HO_2(Ala)_4(H_2O)_8]Cl_6$ (Ala = alanine). Acta Physico-Chimica Sinica. 2003;**19**(5):445–449

[22] Yu HG, Liu Y, Tan ZC, Dong JX, Zou TJ, Huang XM, et al. A solution-reaction isoperibol calorimeter and standard molar enthalpies of formation of $Ln(hq)_2Ac$ (Ln = La, Pr). Thermochimica Acta. 2003;**401**(2):217–224

[23] Lan XZ, Tan ZC, Liu BP, Nan ZD, Sun LX, Xu F. Low-temperature heat capacity and thermal decomposition of crystalline $[Er_2(His\cdot H+)(H_2O)_8]$ $(ClO_4)_6\cdot 4H_2O$. Thermochimica Acta. 2004;**416**(1-2):55–58

[24] Wu XM, Song YJ, Tan ZC, Qu SS. Measurement of low-temperature heat capacity and standard enthalpy of formation of praseodymium glycin perchlorate complex. Chinese Journal of Chemical Physics. 2005;**18**(2):284–288

[25] Di Y-Y, Tan ZC, Li Y-S. Low-temperature heat capacities and thermochemistry of the complex of praseodymium perchlorate with L-alpha-glutamic acid: $[Pr_2(Glu)_2(ClO_4)$ $(H_2O)_7](ClO_4)_3\cdot 4H_2O$. Acta Chimica Sinica. 2006;**64**(13):1393–1401

[26] Wu XM, Tan ZC, Lv XC, Qu SS. Synthesis, heat capacity and enthalpy of formation of $[Ho_2(L\text{-}Glu)_2(H_2O)_8]$ $(ClO_4)_4 \cdot H_2O$. Thermochimica Acta. 2006;**441**(2):199–202

[27] Wu XM, Qu CS, Qu SS, Tan ZC. Low-temperature heat capacity and standard entralpy of formation of neodymium glycine perchlorate complex $[Nd_2(Gly)_6(H_2O)_4(ClO_4)_6 \cdot 5H_2O$. Journal of Thermal Analysis and Calorimetry. 2007;**90**(2):569–573

[28] Zhang JN, Tan ZC, Liu BP, Shi Q, Tong B. Low-temperature heat capacities and thermochemistry properties of $Sm(Val)Cl_3 \cdot 6H_2O$. Acta Physico-Chimica Sinica. 2008;**24**(8):1378–1382

[29] Lv X-C, Tan ZC, Gao X-H. Synthesis and thermochemical properties of new ternary lanthanum complex $La(Glu)(Im)_6(ClO_4)_3 \cdot 4HClO_4 \cdot 4H_2O$. Acta Physico-Chimica Sinica. 2009;**25**(10):1945–1950

[30] Wu XM, Li W, Tan Z-C, Qu SS. Heat capacity and thermodynamical properties of the crystal of $[RE_2(Glu)_2(H_2O)_8]$ $(ClO_4)_4 \cdot H_2O$ (RE = Nd, Eu, Dy). Science in China Series B-Chemistry. 2009;**52**(7):862–867

[31] Zhang JN, Wang H, Tan ZC, Liu BP, Shi Q, Tong B. Low-temperature heat capacities of crystalline $Ho(Gly)_3Cl_3 \cdot 3H_2O$ from 78 to 348 K. Journal of Rare Earths. 2009;**27**(6):919–922

[32] Zhang JN, Tan ZC, Liu BP, Shi Q, Tong B. Thermochemical Behavior of Crystalline RE $(Val)Cl_3 \cdot 6H_2O$ (RE = Nd, Er, Val = Valine). Journal of Chemical and Engineering Data. 2009;**54**(2):392–395

[33] Lv XC, Tan ZC, Gao XH, Yang LN. Microcalorimetric study about biological effect of a synthetic complex: $La(Glu)(Im)_6(ClO_{4)3} \cdot 4HClO_4 \cdot 4H_2O$. Thermochimica Acta. 2010;**510**:213–216

[34] Gao XH, Xu P, Duan WC, Lv XC, Tan ZC, Lu Q. Low-Temperature heat capacity and thermodynamic functions of $Ho(NO_3)_3(C_2H_5O_2N)_4 \cdot H_2O$. Acta Physico-Chimica Sinica. 2013;**29**(10):2123–2128

[35] Liu B-P, Tan ZC. Thermodynamic properties of $Nd(Gly)_2Cl_3 \cdot 3H_2O$ and $Pr(Ala)_3Cl_3$ H_2O. Acta Physico-Chimica Sinica. 2013;**29**(1):17–22

[36] Zhang DS, Tan ZC, Liu BP, Huang XB. Thermodynamic study on complex of neodymium with glycine. Journal of Chemical Thermodynamics. 2015;**83**:27–32

[37] Luo GH, Gao XH, Pan L, Lv XC, Tan ZC., Low-temperature molar heat capacities and thermodynamic properties of a new rare earth complex $Er_2(mu\ 2\text{-}Gly)_6(H_2O)_4 \cdot Na_2(ClO_4)_8$ $(H_2O)_2 \cdot 4H_2O$. Journal of Thermal Analysis and Calorimetry. 2016;**126**(2):871–879

[38] Pan L, Gao XH, Lv XC, Tan ZC. Low-temperature molar heat capacity and thermodynamic properties of rare earth complex. $[EuCu_6(mu\text{-}OH)_3(Gly)_6Im_6](ClO_4)_6 \cdot 3H_2O$. Journal of Thermal Analysis and Calorimetry. 2016;**124**(1):429–435

[39] Nakamoto K. Infrared Spectra of Inorganic and Coordination Compounds. 4th ed. New York: John Wiley & Sons Inc; 1986. p. 258

[40] Wayda AL, Kaplan ML. Mixed ligand imidazole complexes of organolanthanides. Polyhedron. 1990;**9**:751–756

[41] Tan ZC, Shi Q, Liu BP, Zhang HT. A fully automated adiabatic calorimeter for heat capacity measurement between 80 and 400 K. Journal of Thermal Analysis and Calorimetry. 2008;**92**(2):367–374

[42] Donald GA. Thermodynamic properties of synthetic sapphire standard reference material 720 and the effect of temperature- scale difference on thermodynamic properties. Journal of Physical and Chemical Reference Data. 1993;**22**:1441–1452

[43] Yukawa Y, Igarashi S, Masuda Y, Oguni M. Phase transition and glass transition concerning configurational order/disorder of ions in crystalline $(TMA)_2[Sr\{Ni(Pro)_2\}_6](ClO_4)_4$ and $(TMA)[Sm\{Ni(Pro)_2\}_6](ClO_4)_4$. Journal of Molecular Structure. 2002;**605**:277–290

[44] Anna MM, Edward M, Łukasz H, Ireneusz N, Ewa Ś, Jacek Ś, Stanisław W. Phase transition, molecular motions, structural changes and low- frequency vibrations in $[Cu(NH_3)_5](ClO_4)_2$. Chemical Physics. 2005;**317**:188–197

[45] Hangam SS, Westrum ER. Heat capacities and thermodynamic properties of globular molecules I. adamantane and hexamethylenetetramine. Thermodynamic Properties of globular Molecules. 1960;**64**:1547–1551

[46] Udowenko AA, Laptash NM, Maslennikova IG. Orientation disorder in ammonium elpasolites. Crystal structures of $(NH_4)_3AlF_6$,$(NH_4)_3TiOF_5$ and $(NH_4)_3FeF_6$. Journal of Fluorine Chemistry. 2003;**124**:5–15

[47] Di YY, Tan ZC, Zhang GQ, Chen SP, Liu Y, et al. Low-Temperature heat capacity and standard molar enthalpy of formation of the complex $Zn(Thr)SO_4H_2O(s)$. Thermochimica Acta. 2003;**400**(1-2):43–49

[48] Liu YP, Di YY, He DH, Kong YX, Yang WW, Dan WY. The Journal of Chemical Thermodynamics. 2010;**42**:513–517

[49] Sober HA. CRC Handbook of Biochemistry. Ohio: Chemical Rubber Co; 1971. B-63

[50] Cox JD, Wagman DD, Medvedev VA. CODATA Key Values for Thermodynamics. New York: Hemisphere Publishing Corp; 1989

[51] 2009 TA Instruments. http://www.tainstruments.com/

[52] Barros N, Feijóo S, Simoni A, Critter SAM, Airoldi C. Interpretation of the metabolic enthalpy changes calculated for microbiol growth reactions in soils J. Therm. Anal. Calorim. 2001;**63**:577–588

[53] Wadsö I. Thermochim. Acta 2002;**394**:305–311

[54] Xie CL, Tang HK, Qu SS. Microcalorimetric study of bacterial growth. Thermochimi. Acta 1988;**123**:33–41